# A hydromechanical relation governing internal stability of cohesionless soil

**Ricardo Moffat and R. Jonathan Fannin**



**Abstract:** Results are presented from permeameter tests involving unidirectional seepage flow through reconstituted specimens of four widely graded cohesionless soils. The onset of instability is defined by a significant decrease in local hydraulic gradient over a relatively short period of time. The novel concept of a hydromechanical path in stress ($\sigma'_{vm}$) – gradient ($i_{jk}$) space is proposed, which describes the response to seepage flow during testing and terminates at the value of critical hydraulic gradient. The path terminus establishes a hydromechanical boundary governing the onset of seepage-induced internal instability in one-dimensional flow. The boundary represents a failure envelope, which is different for each of the four soils tested. A ranking of seepage-induced instability for each soil, from most unstable to least unstable, is found similar, but not identical to, the susceptibility to internal instability determined from empirical analysis of the gradation shape.

*Key words:* seepage, hydraulic gradient, effective stress, internal instability.

**Résumé :** Des résultats d'essais en perméamètre impliquant un écoulement unidirectionnel à travers des échantillons reconstitués de quatre sols sans cohésion à granulométrie étalée sont présentés. Le début de l'instabilité est défini par une diminution significative du gradient hydraulique local sur une période de temps relativement courte. Le nouveau concept d'un cheminement hydromécanique dans l'espace contrainte ($\sigma'_{vm}$) – gradient ($i_{jk}$) est proposé, qui décrit le comportement en écoulement durant l'essai et qui se termine à la valeur du gradient hydraulique critique. Le point final du cheminement établit une frontière hydromécanique qui gère le début de l'instabilité interne causée par l'infiltration en écoulement unidimensionnel. La frontière représente une enveloppe de rupture, qui est différente pour chacun des quatre sols testés. Un classement de l'instabilité causée par l'infiltration pour chaque sol, du plus instable au moins instable, est semblable mais pas identique à la susceptibilité à l'instabilité interne déterminée à partir d'analyses empiriques de la forme de la gradation.

*Mots-clés :* infiltration, gradient hydraulique, contrainte effective, instabilité interne.

[Traduit par la Rédaction]

## Introduction

Design of sand and gravel filters is typically based on Terzaghi's (1939) empirical criteria, which he developed for specialist technical advising on control of seepage flow beneath concrete weirs and through the soil of zoned earthfill dams (Fannin 2008). A review of the basic properties of sand and gravel filters led Sherard et al. (1984, p. 696) to observe that the Terzaghi criteria "apply to base soils that are internally stable." Recognizing that the phenomenon of internal stability results from a loss of small particles due to disturbing influences, such as seepage as well as vibration, Kenney and Lau (1985) conducted a series of laboratory permeameter tests to define a threshold between stable and potentially unstable gradations of cohesionless, compacted filter materials. Discussion of these findings by Sherard and Dunnigan (1986), and also by Milligan (1986), led Kenney and Lau (1986) to refine an empirical criterion based on shape of the grading curve, and thereby define a stability index $(H/F)_{min}$, termed herein a geometric constraint.

Importantly, Kenney and Lau (1985, p. 225) found "materials that exhibit unstable gradings in these tests show their potential for instability, but whether or not they would behave as unstable materials in practice would depend on the conditions of particle transport to which they were subjected." In other words, if material susceptibility to seepage-induced instability is governed by a geometric constraint arising from the shape of the grain-size distribution curve, it follows that the onset of instability may be deemed subject to a hydromechanical constraint arising from the nature of the seepage regime in the soil.

Yet the hydromechanical influences governing the onset of instability are not well understood. Skempton and Brogan (1994) postulated a relation between $(H/F)_{min}$ and critical hydraulic gradient to trigger the onset of instability (Fig. 1) from laboratory permeameter testing of four sand and gravel mixes. Tests were performed with upward seepage flow and with no confining stress applied to the top surface of the specimen. The critical hydraulic gradient associated with onset of instability was defined as that which causes a disproportionate increase in seepage flow and attributed to a

Received 21 September 2009. Accepted 17 May 2010. Published on the NRC Research Press Web site at cgj.nrc.ca on 1 March 2011.

**R. Moffat.** University of Chile, Blanco Encalada 2002, Santiago, Región Metropolitana, Chile.
**R.J. Fannin.**[1] The University of British Columbia, 6250 Applied Science Lane, Vancouver, BC V6T 1Z4, Canada.

[1]Corresponding author (e-mail: jonathan.fannin@ubc.ca).

**Fig. 1.** Tentative relation of critical gradient and stability index (after Skempton and Brogan 1994).

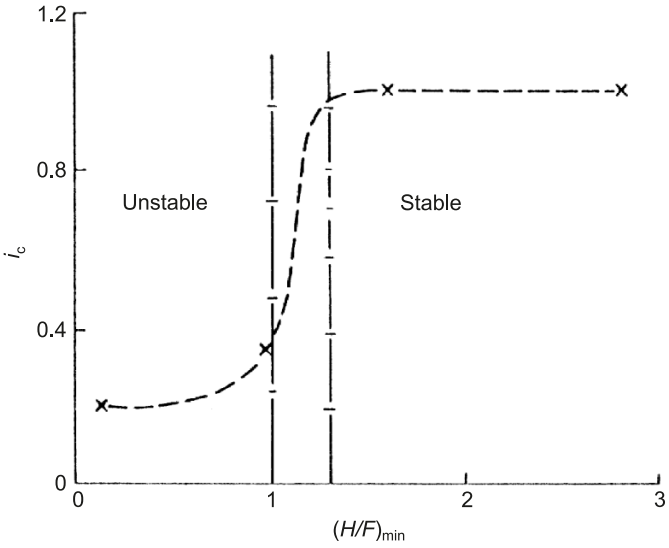


change in hydraulic conductivity of the soil. The experimental finding implies a tentative relation between the geometric and hydromechanical constraints governing internal instability, which led Skempton and Brogan (1994, p. 459) to conclude "further work is required to define more closely the relation of critical gradient and stability index … and to study the effects of varying the density of packing and the proportions of sand to gravel." In a review of hydraulic criteria based on gradient, including the contribution of seepage velocity to sediment transport, Perzlmaier et al. (2007) observed that use of an average hydraulic gradient will not yield the same precision as a value of local hydraulic gradient at the point where the onset of instability occurs.

The objective of this study is to describe the relation between critical hydraulic gradient and stability index in soil that is representative of the core and transition zones, respectively, of the WAC Bennett Dam in British Columbia. A "working hypothesis" to explain the sinkhole events at the dam includes the likelihood that seepage-induced internal erosion took place in the transition and core of the dam (Stewart and Garner 2000; Muir Wood 2007; Garner and Fannin 2010). Accordingly, laboratory permeameter tests were performed on the soils, with seepage flow in either the downward or upward direction. The configuration of the permeameter device (Moffat and Fannin 2006) enables the relation between local hydraulic gradient and effective stress to be characterized, within discrete zones of the test specimen, at the onset of instability. Interpretation of the response to seepage flow takes into account the distinct phenomena of suffusion, suffosion, and piping (Moffat et al. 2011). More generally, findings of the experimental study are intended to advance a broader appreciation for the influence of spatial variations in effective stress, and temporal variations in hydraulic gradient, on the potential for internal instability within zoned earthfill dams.

## Experimental study

A series of laboratory permeameter tests was performed on four widely graded cohesionless soils, for which material properties are reported in Table 1. Two soil types (C-20 and C-30) are representative of the core zone of the W.A.C. Bennett Dam, a silty sand (SM) material according to the American Society for Testing and Materials (ASTM) D2487 Unified Soil Classification System (USCS) (ASTM 2006), which has a fines content of approximately 30%. The other two soil types (T-0 and T-5) are representative of the transition zone that is located immediately downstream of the core, a zone that was constructed with a fines content of approximately 5%. They classify as GP and GP–GM, respectively (where GP is poorly graded gravel and GM is silty gravel), according to the USCS.

The shape of the grain-size distribution curve for each soil yields values of $(H/F)_{min}$ and $(D'_{15}/d'_{85})_{max}$ that are also reported in Table 1. All four soils are deemed internally unstable according to the empirical method of Kenney and Lau (1986) given a stability index $(H/F)_{min} < 1$ and, likewise, they are all deemed internally unstable according to the empirical method of Kezdi (1979) given a filter ratio $(D'_{15}/d'_{85})_{max} > 4$ (Moffat et al. 2011). Strictly speaking, the C-20 and C-30 soils contain an appreciable fines content that renders them outside the scope of the two empirical methods, which were developed for evaluation of coarse-grained soil. However, index testing established the fines fraction of the C-20 and C-30 soil as nonplastic silt; hence, application of the two empirical methods has been extended to characterize the widely graded gravel, sand, and silt of the core material. The evaluation indicates that soil of the transition zone is relatively more susceptible to seepage-induced internal instability than the core of the dam.

A detailed description of the test device, and also the method of specimen reconstitution, has been given by Moffat and Fannin (2006). The device comprises a permeameter cell that mounts in a reaction frame, an axial loading system, a hydraulic control system that imposes unidirectional seepage flow, and a data acquisition system. The rigid-wall permeameter is made of acrylic tubing, and accommodates a cylindrical test specimen that is 279 mm in diameter. The soil is reconstituted as a saturated slurry (Fig. 2*a*), consolidated under the influence of a constant vertical effective stress ($\sigma'_{to}$) applied to the top surface of the specimen (Fig. 2*b*), and then subject to unidirectional seepage flow in either a downward or an upward direction (Fig. 2*c*). The method of specimen reconstitution by consolidation of saturated slurry used in the laboratory differs from the method of placement by compaction of partially saturated fill used in construction of the dam. The laboratory method was used because of the confidence it imparts to interpretation of test data using the principle of effective stress. Specimen length measured at end-of-consolidation is reported in Table 2.

The variation of local hydraulic gradient ($i_{jk}$) is deduced from measurement of pore-water pressure at ports located along the length of the specimen at a vertical spacing of 125 mm (Fig. 2*a*). The average vertical effective stress ($\sigma'_{vm}$) between two adjacent port locations is then determined knowing $\sigma'_t$, $i_{jk}$, and $\sigma'_b$ (Moffat 2005): initial values of $\sigma'_{to}$ and $\sigma'_{bo}$ are established from top and bottom load cell measurements, respectively, and used to determine the corresponding vertical total stress, knowing the pore-water pressure measured at each boundary. Vertical total stress is assumed to vary linearly along the length of the specimen,

**Table 1.** Properties and stability index values of soil used in testing.

| Soil type | Fines content (% < 74 μm) | $D_{85}$ (mm) | $D_{60}$ (mm) | $D_{50}$ (mm) | $D_{10}$ (mm) | $(D'_{15}/d'_{85})_{max}$ at $F$ (%) | $(H/F)_{min}$,[a] $F < 0.2$ | $(H/F)_{min}$,[b] $F < 0.3$ |
|---|---|---|---|---|---|---|---|---|
| T-0 | 0 | 38.5 | 11 | 7.4 | 0.15 | 13.7 at 30% | 0.95 | 0.29 |
| T-5 | 5 | 38.5 | 11 | 7.4 | 0.13 | 14.3 at 30% | 0.9 | 0.29 |
| C-20 | 20 | 3.4 | 0.6 | 0.42 | 0.021 | 7.7 at 5% | 0.67 | 0.67 |
| C-30 | 30 | 3.0 | 0.6 | 0.42 | 0.018 | 10 at 5.6% | 0.67 | 0.42 |

[a]Kenney and Lau (1986) method.
[b]Modified Kenney and Lau (1986) method.

**Fig. 2.** (*a*) Arrangement of the test specimen, and idealized profile of vertical effective stress under (*b*) no flow and (*c*) unidirectional seepage flow. DPT, differential pressure transducer; LVDT, linear variable differential transformer; TPT, total pressure transducer.

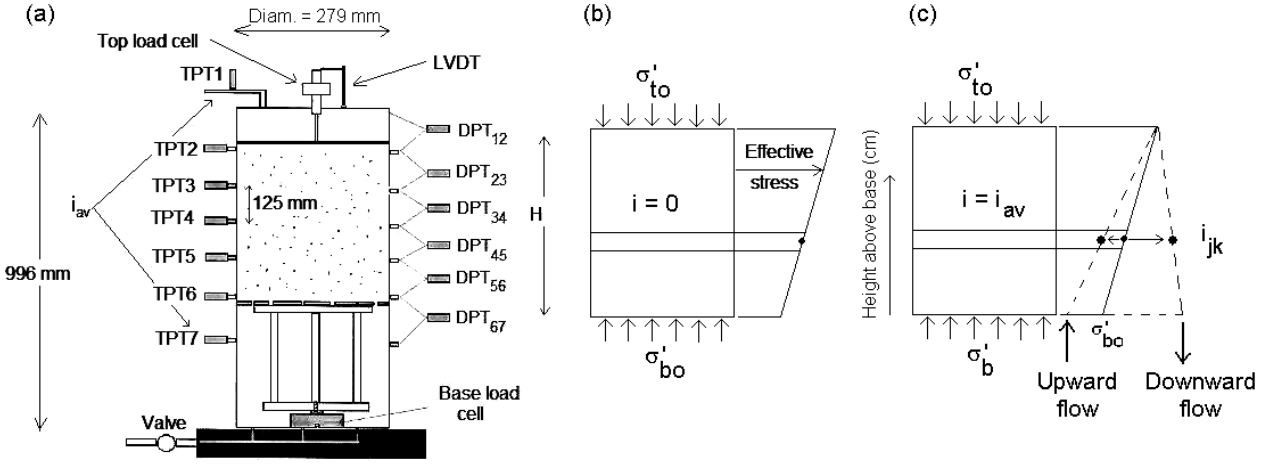


**Table 2.** Summary of test results.

| Test code | $e_c$ | Specimen length (cm) | $i_{av}$ | Port location of failure | $i_{cr}$ | $\sigma'_{vm}$ (kPa) |
|---|---|---|---|---|---|---|
| T-0-25-D | 0.38 | 55.2 | 11 | 56 | 7 | 38 |
| T-0-100-D | 0.33 | 55.5 | 8 | 45 | 12 | 62 |
| T-0-175-D | 0.33 | 55.6 | 45 | 56 | 25 | 183 |
| T-5-25-D | 0.28 | 44.2 | — | No failure | — | — |
| T-5-175-U | N.A. | 44.0 | 31 | 34 | 38 | 139 |
| T-5-50-D | 0.29 | 45.0 | 11 | 45 | 18 | 58 |
| T-5-50-D-R | N.A. | 42.4 | 36 | 56 | 57 | 106 |
| T-5-25-U | 0.30 | 45.5 | 6 | 23 | 13 | 23 |
| T-5-30-U | 0.29 | 45.0 | 13 | 35 | 23 | 41 |
| C-20-50-U | 0.37 | 34.0 | 27 | 56 | 35 | 25 |
| C-20-85-U | 0.39 | 34.5 | 37 | 56 | 25 | 21 |
| C-30-25-U | 0.44 | 35.5 | 13 | 45 | 15 | 16 |
| C-30-50-U | 0.44 | 35.4 | 14 | 56 | 16 | 21 |
| C-30-80-U | 0.36 | 33.5 | 29 | 45 | 39 | 41 |
| C-30-100-U* | 0.39 | 32.5 | 28 | 56 | 18 | 19 |

**Note:** N.A., not available.
*Stress-controlled test.

allowing calculation of $\sigma'_{vm}$ (to a resolution of ±0.5 kPa) knowing the magnitude of $i_{jk}$ (to a resolution of ±0.5).

## Test procedure and program

Variables examined in the program of testing were soil type (T-5, T-0, C-30, and C-20), vertical effective stress applied to the top surface of the soil specimen (25 to 175 kPa), hydraulic gradient across the specimen, and direction of seepage flow in the permeameter (upward or downward). Accordingly, test code T-0-25-D (see Table 2) describes a specimen of T-0 soil, consolidated to $\sigma'_{to}$ = 25 kPa, and then subjected to seepage flow in the downward direction. A test was terminated when the onset of instability was encountered or, in the case of test T-5-25-D, when the capacity of the permeameter was exceeded.

All tests except one were performed with gradient-controlled seepage at constant vertical effective stress on the top boundary, wherein the soil was consolidated to a target value of $\sigma'_{to}$ and then subjected to unidirectional

seepage flow at increasing values of $i_{av}$ across the test specimen, with $\sigma'_{to}$ held constant. Typically, the gradient was raised in increments of $\Delta i_{av} = 1$, until the onset of instability occurred or the capacity of the device was exceeded. The duration of each stage was typically 90 min, with occasional stages of longer duration to allow for sufficient volumetric discharge to determine a value of hydraulic conductivity for the C-30 and C-20 soils. In contrast, it was decided to consolidate one specimen of core material (test C-30-100-U) to a target value $\sigma'_{to}$ = 100 kPa and subject it to upward seepage flow at increasing gradient to $i_{av} = 28$ with $\sigma'_{to}$ held constant, whereupon a stress-controlled unloading of the top of the specimen was then imposed at a constant value of hydraulic gradient, namely $i_{av} = 28$. The objective of this one stress-controlled test was to compare the response of the C-30 soil with three other gradient-controlled tests on the same soil (see Table 2), thereby evaluating the relation between critical gradient and effective stress with reference to a different hydromechanical path leading to the onset of instability. The novel concept of a hydromechanical path, as it relates to interpretation of these permeameter test data, follows directly from the variation of effective stress that occurred in response to the hydraulic gradient imposed during a test, and is described below.

## Test results

It is postulated the spatial variation of effective stress and hydraulic gradient will govern the location where onset of particle migration occurs in a soil that, as a consequence of the shape of its grain-size distribution curve, is rendered susceptible to internal instability. Accordingly, particular emphasis was placed on establishing the magnitude of $\sigma'_{vm}$ and $i_{jk}$ during permeameter testing, at different locations along the length of the specimen. Recognizing that the onset of instability is a localized phenomenon (Perzlmaier et al. 2007), it is reasonable to expect that the exact location at which it occurs within the permeameter may vary from one test specimen to another.

### Spatial variation of effective stress

Consider the idealized response of a soil element to consolidation and unidirectional seepage flow. The test specimen was consolidated to a target vertical effective stress on the top boundary ($\sigma'_{to}$), yielding a vertical effective stress at the lower boundary ($\sigma'_{bo}$) that is smaller as a consequence of frictional losses along the inside wall of the permeameter cell (Fig. 2*b*). In a test with gradient-controlled seepage at constant $\sigma'_{to}$, imposition of downward flow causes the vertical effective stress to increase due to the action of seepage force in the soil while, in contrast, upward flow causes a reduction in effective stress (Fig. 2*c*). Ideally, prior to the onset of instability in a perfectly homogeneous specimen, the average hydraulic gradient ($i_{av}$) would equal the local hydraulic gradient ($i_{jk}$) along the entire length of the specimen, as shown schematically in the diagram.

#### *Transition materials*

Three tests were performed on the T-0 gradation, for which the reconstituted soil was consolidated to $25 \le \sigma'_{to} \le 175$ kPa; all test specimens were subjected to downward seepage flow (Table 2). Test T-0-25-D has been selected to illustrate the variation of effective stress at each port location along the length of the specimen (Fig. 3*a*). The "initial" relation describes the change in $\sigma'_v$ along the specimen at the end of consolidation: it is linear as a consequence of the assumed variation of total stress between known values at the top and bottom boundary, and the linear increase of pore-water pressure with depth for the prevailing hydrostatic condition ($i_{av} = 0$), at that stage of the test. The reduction in vertical effective stress that occurs with depth is attributed to interface friction between the soil specimen and the inside wall of the permeameter. The resultant arching within the soil yields a significant influence in all tests: this experimental finding confirms the importance of measuring the reaction force on the base of the specimen (see Fig. 2*a*), in support of any stress-based interpretation of the response to seepage flow. Downward seepage flow in test T-0-25-D generated an increase in vertical effective stress, which was detected as a reduction in pore-water pressure at port locations along the permeameter wall. The increase is attributed to viscous friction producing a frictional drag, or seepage force, which acts in the direction of flow. The relation termed "onset" is the one obtained immediately prior to the occurrence of seepage-induced instability in the final stage of the test: it is nonlinear, a response that is attributed to spatial variations in hydraulic conductivity within the specimen yielding a nonlinear distribution of pore-water pressure with depth in response to the imposed seepage flow.

Six tests were performed on the T-5 gradation, with consolidation to the same stress range of $25 \le \sigma'_{to} \le 175$ kPa (see Table 2). Three of the specimens were subjected to downward flow (test T-5-50-D was repeated, and termed T-5-50-D-R), and three were subjected to upward flow. All specimens exhibited an onset of instability, except T-5-25-D for which the capacity of the permeameter to apply sufficient hydraulic gradient was exceeded. Two tests have been selected to illustrate the variation of effective stress in soil T-5, one with downward flow and the other with upward flow. Downward flow caused the effective stress to increase for T-5-50-D (Fig. 3*a*), yielding a nonlinear variation that is comparable in shape to that observed for T-0-25-D. In contrast, upward flow in the T-5-175-U specimen generated a decrease in effective stress, evident for example in the stage at an average hydraulic gradient across the full length of the specimen $i_{av} = 25$ (Fig. 3*b*). Additional increments of hydraulic gradient caused the effective stress to vary in a complex and somewhat unexpected manner just prior to the onset of instability, with the onset at $i_{av} = 31$ exhibiting a slight increase in effective stress at the base (inlet) of the specimen.

#### *Core materials*

All tests on core materials were conducted with upward seepage flow. Two tests were performed on the C-20 gradation, for which the reconstituted soil was consolidated to $\sigma'_{to}$ = 50 and 85 kPa and the specimen was then subjected to multi-stage seepage flow (Table 2). Test C-20-50-U has been selected to illustrate the variation of effective stress along the specimen (Fig. 4*a*). The "initial" relation again

**Fig. 3.** (*a*) Profiles of vertical effective stress with depth: soil tests T-0-25-D and T-5-50-D. (*b*) Profiles of vertical effective stress: test T-5-175-U.

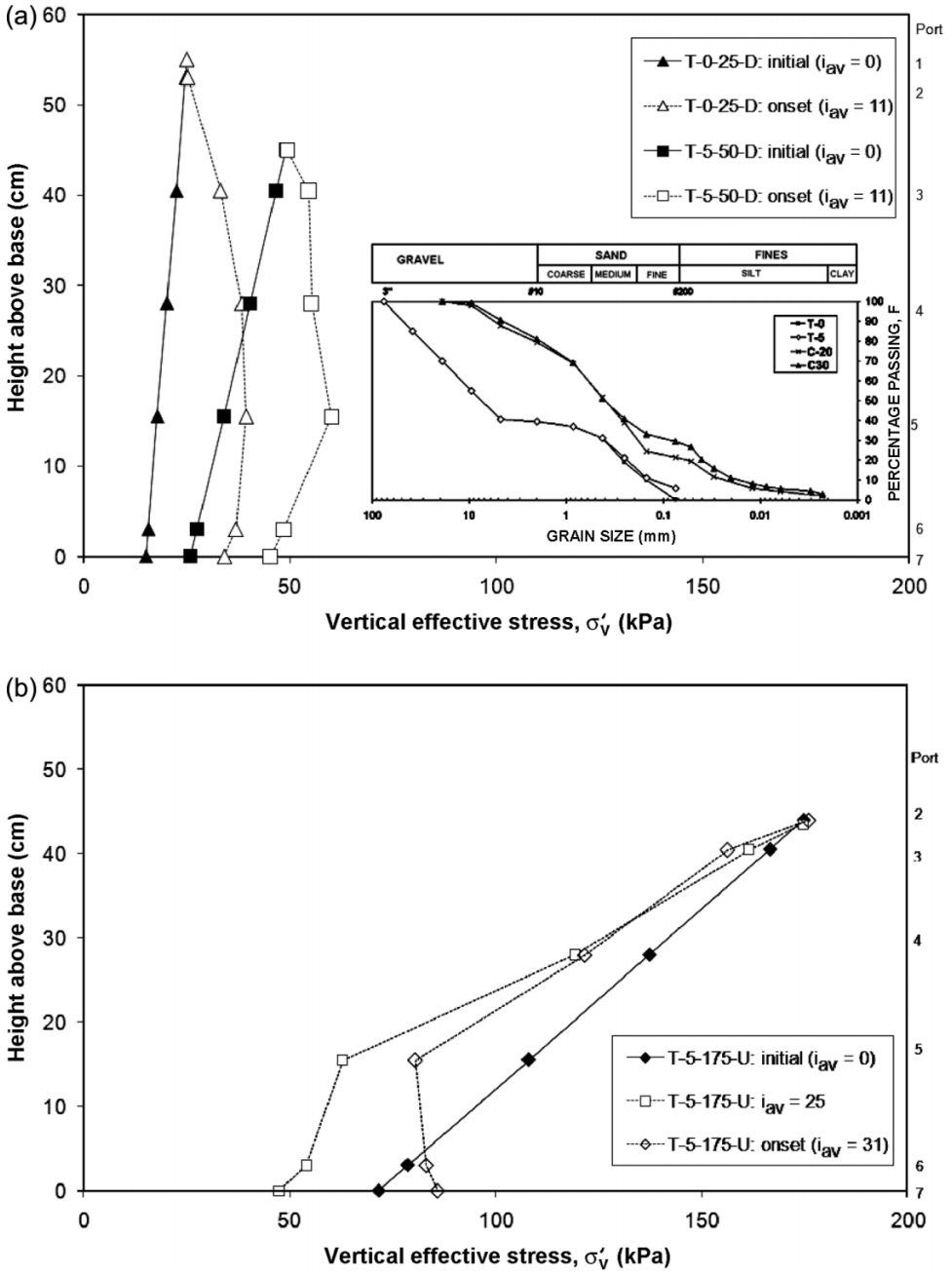


exhibits a significant reduction of $\sigma'_v$ with depth that is attributed to the action of sidewall friction. In subsequent stages with upward flow, occasional manual adjustment of the control system was found necessary to target a constant value of $\sigma'_{to}$, and the very small increase in $\sigma'_{to}$ between the "initial" and "onset" condition while the test was in progress is attributed to this adjustment. Upward flow, and the consequent seepage force, yields a reduction in effective stress that is evident, for example, in the lower portion of the specimen at $i_{av} = 21$. However, the data reveal effective stress that varied in a complex and somewhat unexpected manner as the specimen approached failure, with the stage at $i_{av} = 21$ also yielding an increase in effective stress in the upper portion of the specimen that remained through to the onset of instability at $i_{av} = 27$. The response is tentatively attributed to interaction between the mobilized seepage force and the stress-controlled top boundary in a soil that is demonstrated, through analysis reported below, to be the least susceptible to internal instability.

Four tests were performed on the C-30 gradation, with consolidation to $25 \leq \sigma'_{to} \leq 80$ kPa in three tests conducted with gradient-controlled seepage at constant $\sigma'_{to}$ (Table 2). Test C-30-80-U has been selected to illustrate the variation of effective stress at each port location (Fig. 4*b*). Once again, the influence of manual adjustment of the control system is evident from the increase of $\sigma'_{to}$ that occurred be-

**Fig. 4.** Profiles of vertical effective stress: (*a*) test C-20-50-U and (*b*) tests C-30-80-U and C-30-100-U.

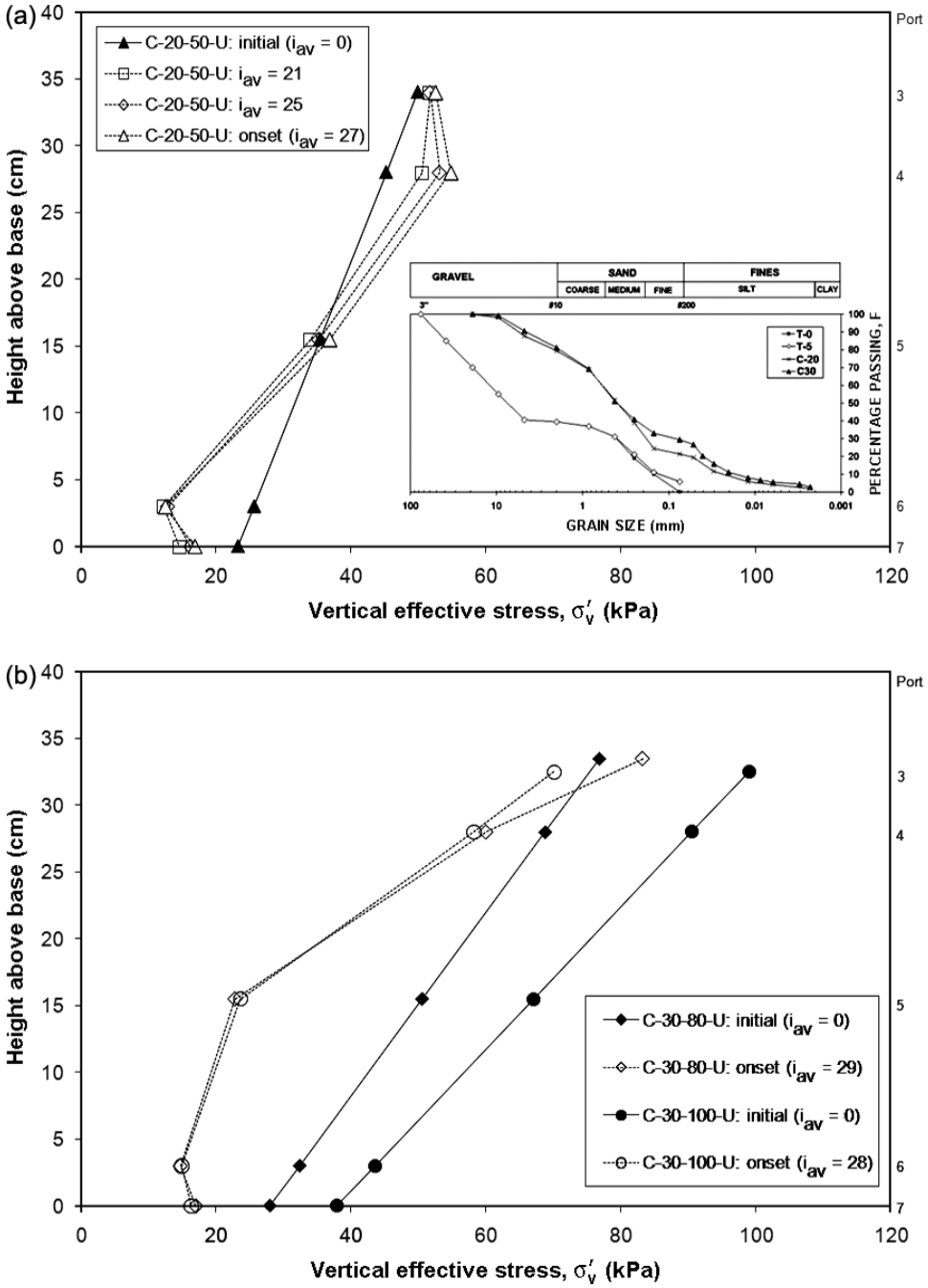


tween the "initial" and "onset" conditions, a change from 77 to 83 kPa, respectively. Inspection of the data for the onset condition shows a decrease in effective stress throughout the specimen length that, like all the other tests, confirms a nonlinear variation of effective stress with depth. As noted earlier, one C-30 specimen was consolidated to $\sigma'_{to}$ = 99 kPa, in a test for which the onset of instability was subsequently triggered by means of stress-controlled unloading of the top of the specimen. The data for that C-30-100-U specimen (Fig. 4*b*) depict this relatively significant reduction in $\sigma'_{to}$ from an "initial" value of 99 kPa at $i_{av}$ = 0 to a value of 70 kPa immediately prior to the "onset" of instability at $i_{av}$ = 28. Comparison of the four tests with upward flow (Fig. 3*b*, and Figs. 4*a* and 4*b*) indicates a general nonlinear variation of $\sigma'_v$ with depth, at onset of instability, which is the inverse of that for the tests with downward flow (Fig. 3*a*). The response is tentatively attributed to the influence of a stress-controlled top boundary and a strain-controlled (zero strain) lateral and bottom boundary.

## Hydraulic gradient at the onset of instability

The spatial and temporal progress of internal instability has been described in detail with reference to four tests that were selected for illustrative purposes (Moffat et al. 2011). The four tests were performed on two transition materials (T-0-25-D and T-5-175-U) and two core materials (C-20-

50-U and C-30-80-U); namely, the same four tests for which the profile of vertical effective stress has now been described in Figs. 3 and 4. The corresponding temporal variation of local hydraulic gradient leading up to the onset of instability in these four tests is reproduced in Fig. 5. Recall that Perzlmaier et al. (2007) acknowledge the utility of such local measurement of hydraulic gradient, and the capacity to record these data has proven a very beneficial aspect of the permeameter design.

The local hydraulic gradient is calculated from the distribution of water head along the length of the specimen, using the array of total pressure transducers (TPT) and differential pressure transducers (DPT) located on opposite sides of the permeameter (Fig. 2*a*). Inspection of the relation between $i_{jk}$ and time yields a value for the local hydraulic gradient just prior to instability occurring (Fig. 5), termed the critical hydraulic gradient, $i_{cr}$, herein. Onset of instability is deemed to occur within soil between any two port locations where a significant decrease in $i_{jk}$ is first recorded. For example, inspection of the data for test T-0-25-D yields $i_{cr} = 7$ within a localized zone between ports 5 and 6 on the permeameter (Fig. 5*a*). The resulting values of $i_{cr}$ are reported for all tests in Table 2, together with the two port locations that define where the onset occurred locally within the specimen and, for purposes of clarity, the average hydraulic gradient $i_{av}$ imposed across the complete length of the specimen in that final stage of the test.

## Analysis

The variation of local hydraulic gradient ($i_{jk}$) across the two port locations where onset of instability was found to occur, and the resulting change in vertical effective stress at the mid-point elevation between the two ports ($\sigma'_{vm}$), yield a relation that may be plotted in stress–gradient space. The relation establishes a "hydromechanical" path. It describes the response of the test specimen to seepage flow, and it terminates at the value of critical hydraulic gradient established locally within the specimen. For example, the stress–gradient relation for test T-0-25-D between ports 5 and 6 commences with the initial hydrostatic condition of $i_{56} = i_{av} = 0$ and $\sigma'_{vm} = 17$ kPa (see Fig. 3*a*), and progresses to terminate at values of $i_{av} = 11$ and $\sigma'_{vm} = 38$ kPa that are associated with the onset of instability at $i_{56} = i_{cr} = 7$ (see Figs. 3*a*, 5*a*, and Table 2), yielding the hydromechanical path depicted in Fig. 6. Inspection of the terminal point for T-0-25-D, and corresponding terminal points for the companion T-0-100-D and T-0-175-D tests, suggests a trend of increasing critical hydraulic gradient with increasing effective stress. The trend is described by a linear fit to the average of the three terminal values that is taken, for purposes of simplicity, through the origin of the axes. The simplification of a zero intercept is further discussed below. The "average" fit defines an approximate boundary to the onset of instability in the T-0 soil. For any value of effective stress $\sigma'_{vm}$, the boundary establishes the critical gradient $i_{cr}$, together with a permissible stress–gradient zone below that boundary wherein the soil is stable. Data scatter is illustrated by means of a "minimum" and "maximum" envelope plotted through the corresponding values of $i_{cr}$ found in testing. In theory, the relation between stress and gradient should define a unique envelope, and the data scatter is tentatively attributed to the constraint of using fixed port locations to determine values of local hydraulic gradient over a relatively long gauge length of 125 mm (see Fig. 2), and also to uncertainty in the calculation of $\sigma'_{vm}$ at the mid-point elevation between port locations.

A total of six tests were performed on the T-5 soil (see Table 2). The hydromechanical path obtained in four of those tests is illustrated in Fig. 7. The tests include specimens subjected to downward and also upward flow. Inspection of the terminal points suggests a trend of increasing critical hydraulic gradient with increasing stress that is again described by a linear fit to the average of the four values, through the origin of the plot, which defines an approximate boundary to the onset of instability in the T-5 soil. Although T-5-50-D(R) did exhibit internal instability, the path is not illustrated because this particular test involved a re-use of the intact, but previously tested, T-5-50-D specimen. It is encouraging, however, that the values of $i_{cr} = 57$ and $\sigma'_{vm} = 106$ (see Table 2) locate the terminus for the repeated test within the minimum–maximum range of the other four tests. The capacity of the permeameter was exceeded before test T-5-25-D exhibited any internal instability: the end-of-test value for the central zone of the test specimen ($i_{46}$) is found to plot below the "average" fit for the T-5 soil (see Fig. 7), very close to the "minimum" envelope, suggesting the specimen may have been approaching a condition of instability.

Three tests were performed on the C-30 soil using gradient-controlled seepage (see Table 2), for which the hydromechanical paths are illustrated in Fig. 8. Once again, the same general trend of increasing critical hydraulic gradient with increasing effective stress is apparent in the data. It is described by a linear fit to the average of the three terminal values, taken through the origin of the plot, which defines an approximate boundary to the onset of instability in the C-30 soil. As before, a "minimum" and "maximum" envelope to the data is included on the plot, to illustrate the scatter in measured values. The "average" fit is reproduced in Fig. 9 together with data from the C-30-100-U test that was performed with stress-controlled unloading of the specimen. It proved very difficult to distinguish the exact location where onset of instability was triggered within the central portion of this specimen, from analysis of the spatial and temporal variation of effective stress; therefore, the hydromechanical path is reported for the soil between ports 4 and 5 and also between ports 5 and 6. The abrupt change in shape of the $\sigma'_{vm}$ versus $i_{jk}$ relation occurs at the stage in testing where stress-controlled unloading commenced, at the constant value $i_{av} = 28$. The two curves both diminish to a terminal point defined by a local value of hydraulic gradient, and corresponding effective stress, which is in excellent agreement with the "average" fit established from the three gradient-controlled tests (Fig. 9).

Only two tests were performed on the C-20 soil, for which the corresponding hydromechanical paths to onset of instability are given in Fig. 8. Notwithstanding the limited data, a linear fit is shown to the average of the two terminal values, through the origin of the plot, to establish an approximate boundary for the C-20 soil.

**Fig. 5.** Onset of instability in test: (*a*) T-0-25-D ($i_{av}$ = 11); (*b*) T-5-175-U ($i_{av}$ = 31); (*c*) C-20-50-U ($i_{av}$ = 27); (*d*) C-30-80-U ($i_{av}$ = 29).

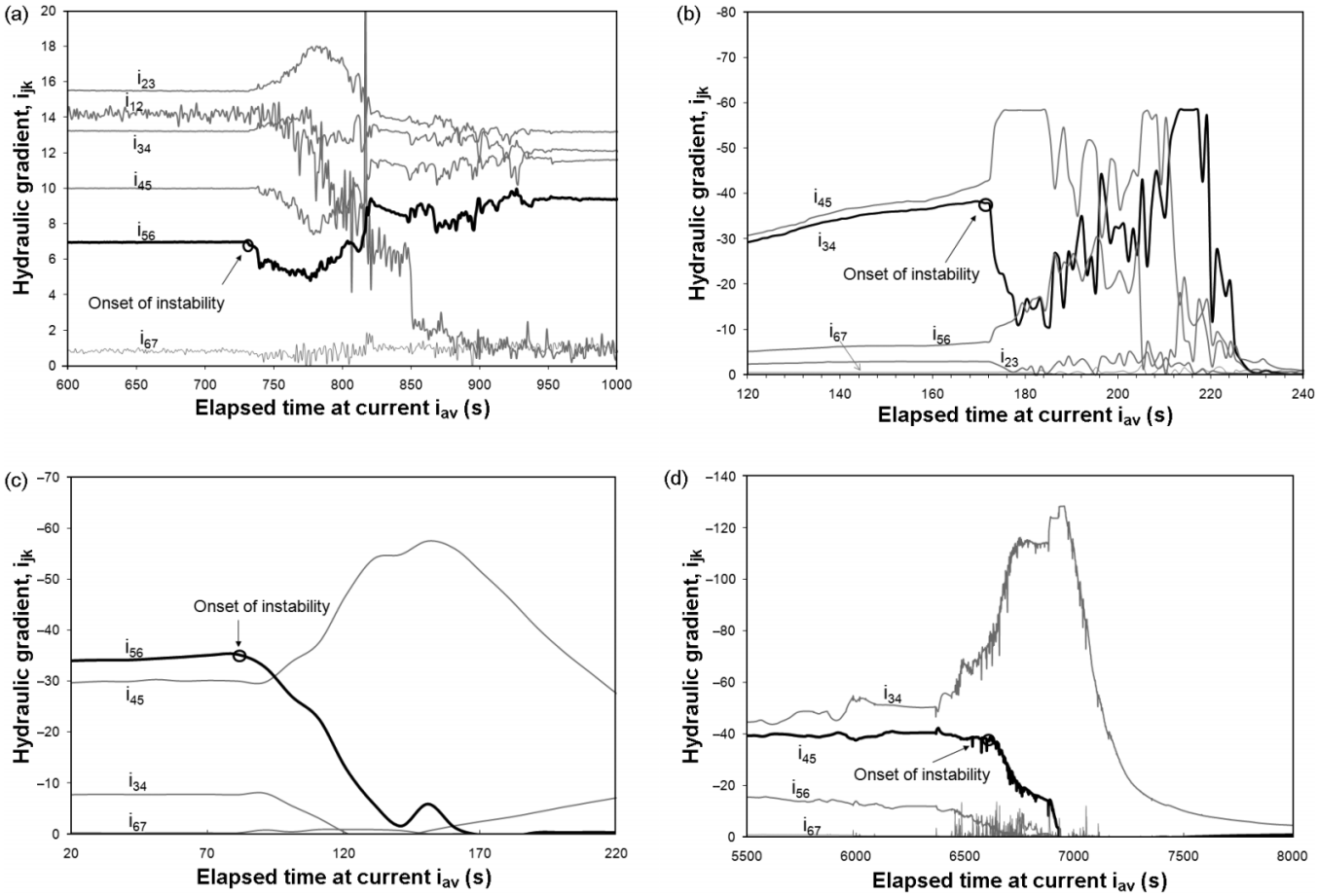


**Fig. 6.** Hydromechanical boundary to internal instability: soil T-0. Av., average.

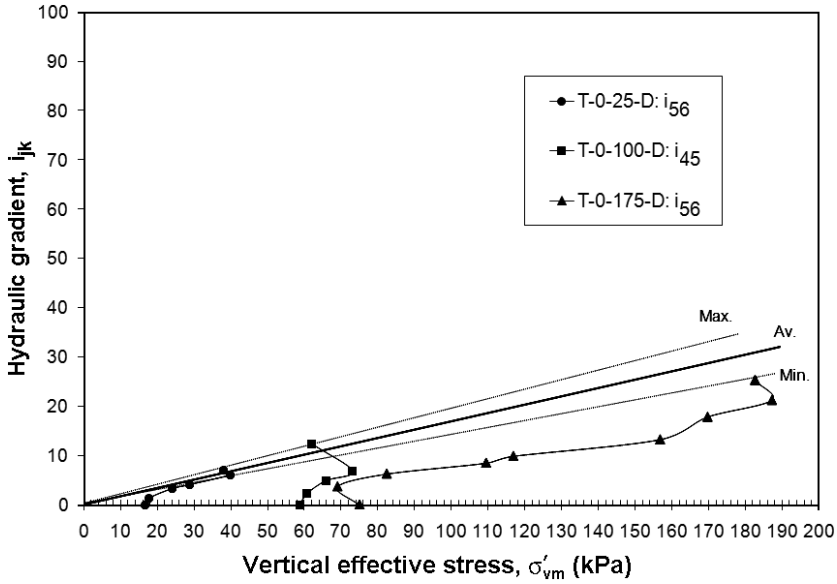


In summary, the relation between local hydraulic gradient and effective stress defines a hydromechanical path to the onset of instability that occurred in 14 of the 15 tests, each of which terminates at a critical hydraulic gradient $i_{cr}$. The path appears bounded by a linear relation in stress–gradient space at which the onset internal instability occurs. More specifically, the relation defines a hydromechanical boundary in $\sigma'_{vm}$–$i_{cr}$ space, below which a soil does not exhibit its potential for instability.

**Fig. 7.** Hydromechanical boundary to internal instability: soil T-5.

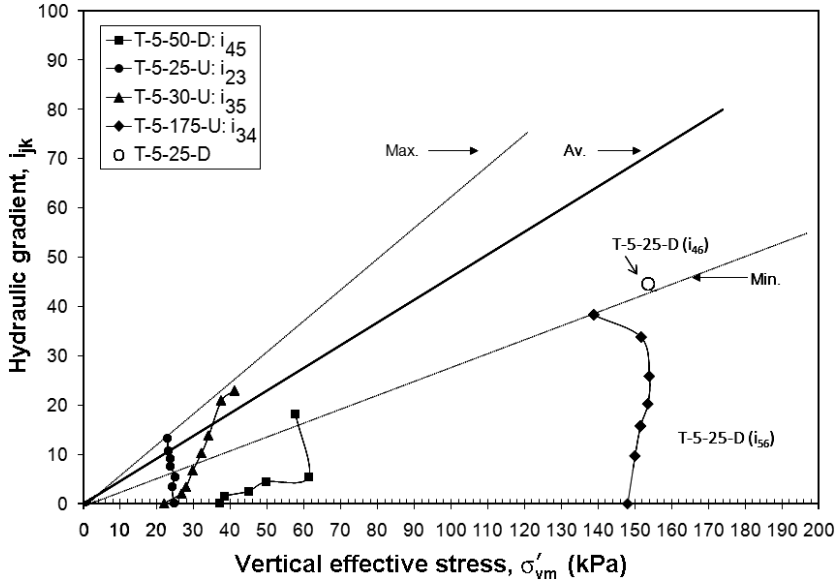


**Fig. 8.** Hydromechanical boundary to internal instability: soils C-20 and C-30.

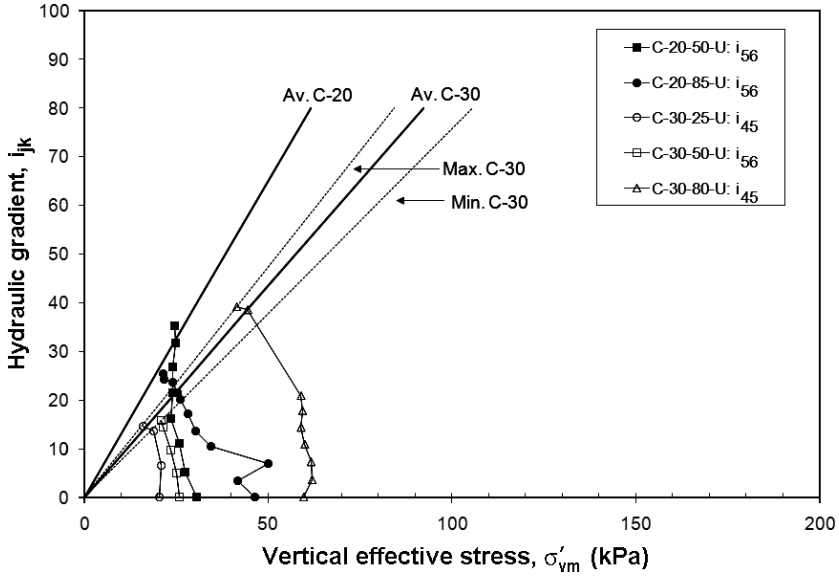


## Discussion

As first noted in the analysis of T-0 test data, the linear fit to values of critical hydraulic gradient is taken arbitrarily through the origin of the plot (see Figs. 6 to 10). Strictly speaking, this is a simplification and the fit should be defined by two parameters; namely, slope of the line and intercept on the $i_{jk}$ axis. Recall the classic study of Terzaghi on uniform sand that is subjected to upward seepage (Terzaghi 1939; Fannin 2008), with no surface loading, for which heave is associated with zero vertical effective stress at a theoretical value for the critical hydraulic gradient of $\gamma'/\gamma_w \approx 1$. Accordingly, soil with a gradation curve that is internally stable will yield a best fit with an intercept on the stress–gradient plot of approximately (0,1). From testing of two sandy gravels that were subjected to upward vertical flow, also with no surface loading, Skempton and Brogan (1994, p. 459) found instability "... of the sand grains can occur at hydraulic gradients one third to one fifth of the theoretical critical gradient." More specifically, the two sandy gravels, with $(H/F)_{min} = 0.14$ and 0.98, yielded a critical hydraulic gradient of 0.2 and 0.34, respectively (see Fig. 1). Therefore, the linear fit should yield an intercept less than or equal to $i_{jk} = i_{cr} = 1$ on the vertical axis and, for purposes of simplicity, each fit to the current study has been taken through the origin (Fig. 10).

The T-5 soil was subjected to seepage flow in both the downward and upward directions. From inspection of the results (Fig. 7), it appears the hydromechanical envelope is independent of the direction of seepage flow, given the onset of instability in a test with downward flow (T-5-50-D) is governed by the same general boundary as three tests with upward flow (T-5-25-U, T-5-30-U, and T-5-175-U). Results obtained for this soil yield the greatest scatter in values of

**Fig. 9.** Influence of effective stress: test C-30-100-U.

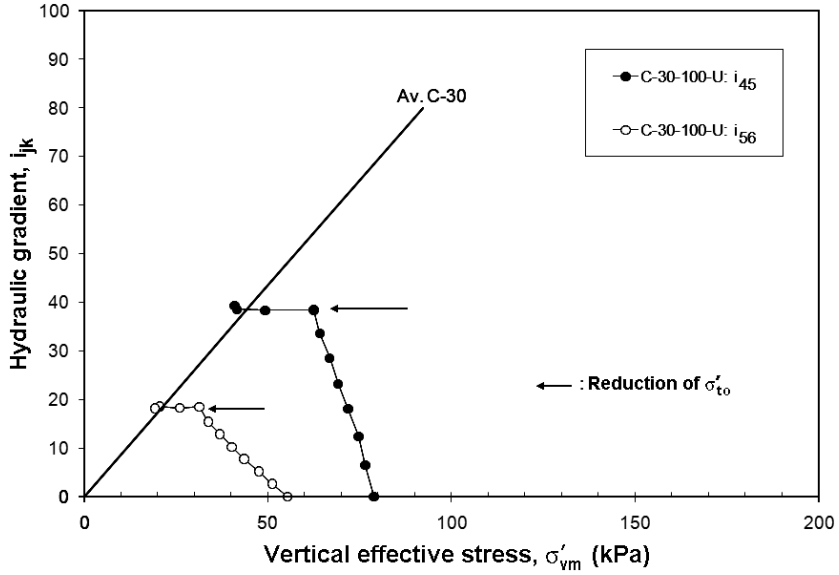


**Fig. 10.** Summary of hydromechanical boundaries in stress–gradient space.

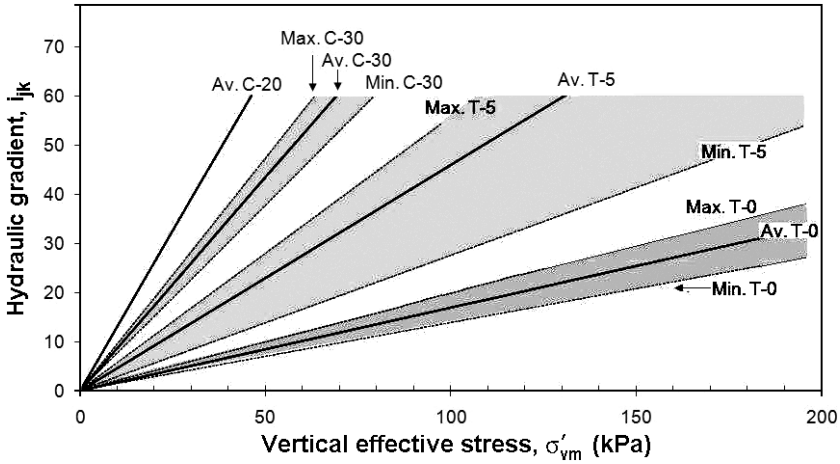


critical hydraulic gradient (Fig. 10). The scatter is tentatively attributed to the difficulty of reconstituting a homogenous specimen of sandy gravel with a very small content of only 5% silt, and the consequent potential for significant spatial variation of grain-size distribution within a test specimen.

Results obtained for the two transition materials indicate the "average" fit for the T-0 soil (Fig. 6) plots below that of the T-5 soil (Fig. 7). Results obtained for both core materials plot above those for the transition materials, with the "average" fit for the C-30 gradation plotting below that for the C-20 gradation (Fig. 8). The finding implies that, at any value of effective stress, initiation of instability requires a larger hydraulic gradient in the core material than the transition material. Accordingly, the slope of the hydromechanical boundary is believed to depend partly on the shape of the gradation curve of each material. As the T-5 soil requires a larger gradient than the T-0 soil, and the C-20 core material requires a larger gradient than the C-30 material, a ranking of the hydromechanical envelope for each soil is obtained as follows: T-0 < T-5 < C-30 < C-20 (see Fig. 10). Inspection of the $(D'_{15}/d'_{85})_{max}$ and $(H/F)_{min}$ at $F < 0.3$ stability indices (see Table 1) establishes that the ranking of plotting position in Fig. 10 is similar, but not identical to, a ranking of the geometrical susceptibility to internal instability given by T-5 < T-0 < C-30 < C-20 (see Table 1).

A "working hypothesis" to explain the sinkhole events at the WAC Bennett Dam includes the likelihood that seepage-induced internal erosion took place in the transition and core of the dam (Stewart and Garner 2000; Muir Wood 2007). Statistical analyses of all gradation curves from the construction records confirm both the transition and core materials of the dam are susceptible to instability (Li et al. 2009), with the transition being the more susceptible material of the two zones. Permeameter testing on reconstituted specimens of the T-5 soil, a gradation selected to represent the transition zone, and the C-30 soil, a gradation selected to represent the core zone in the dam, has established that both of these materials exhibit seepage-induced internal instability in one-dimensional flow. The experimental finding supports the belief that internal instability may have occurred in the dam, at locations where the configuration of these two

zones, the method of construction, and the nature of the seepage-regime yielded a critical combination of effective stress and hydraulic gradient (Garner and Fannin 2010).

## Conclusions

The following conclusions are based on the results of permeameter tests involving unidirectional seepage flow through reconstituted specimens of four widely graded cohesionless soils:

(1) Values of local hydraulic gradient within the test specimen were found extremely useful to an interpretation of the onset of internal instability. The onset of instability is defined by a significant decrease in local hydraulic gradient over a relatively short period of time.

(2) Spatial variations of local hydraulic gradient ($i_{jk}$) and mean vertical effective stress ($\sigma'_{vm}$) govern the location where onset of particle migration occurs in a specimen. The novel concept of a hydromechanical path in stress ($\sigma'_{vm}$) – gradient ($i_{jk}$) space is proposed, which describes the response to seepage flow during testing. The hydromechanical path associated with localized onset of instability terminates at the value of critical hydraulic gradient ($i_{cr}$).

(3) A trend of increasing $i_{cr}$ with increasing $\sigma'_{vm}$ was found, from tests on specimens consolidated to different values of top boundary stress ($\sigma'_{to}$). A linear fit to these $\sigma'_{vm}$ versus $i_{cr}$ data for each soil yields a hydromechanical envelope governing the onset of seepage-induced internal instability in one-dimensional flow. The fit should have an intercept less than or equal to $i_{jk} = i_{cr} = 1$ at $\sigma'_{vm} = 0$.

(4) The onset of internal instability is triggered either by an increase in hydraulic gradient or by a decrease in effective stress. Each trigger yields a similar response, and appears to occur at the same hydromechanical boundary in stress–gradient space.

(5) The slope of the linear fit, and therefore the hydromechanical boundary, is different for each of the four soils tested. A ranking of seepage-induced instability for each soil, from most unstable to least unstable, is given by T-0 < T-5 < C-30 < C-20. It is similar, but not identical, to a ranking of susceptibility to internal instability determined from shape analysis of the corresponding gradation curves that is given by T-5 < T-0 < C-30 < C-20.

(6) Strictly speaking, the C-20 and C-30 soils contain an appreciable fines content that renders them outside the scope of the Kenney and Lau (1985, 1986) empirical method, which was developed from testing of coarse-grained soils with no fines content. Nonetheless, the gradation curves are deemed internally unstable by that method, and have been found internally unstable in the laboratory permeameter tests. The results suggest that this Kenney–Lau method may be applicable to an evaluation of coarse-grained soil with a component of non-plastic silt.

(7) The experimental findings support the hypothesis that sinkhole events at the WAC Bennett Dam may be explained by the phenomenon of seepage-induced internal instability.



## Acknowledgment

The experimental work was conducted in collaboration with the British Columbia Hydroelectric Power Authority, which provided financial support and supplied the soils evaluated in the testing program.

## References

ASTM. 2006. Standard practice for classification of soil for engineering purposes (Unified Soil Classification System). ASTM standard D2487. Annual Book of ASTM Standards. American Society for Testing and Materials, West Conshohocken, Pa.

Fannin, R.J. 2008. Karl Terzaghi: from theory to practice in geotechnical filter design. Journal of Geotechnical and Geoenvironmental Engineering, **134**: 267–276.

Garner, S.J., and Fannin, R.J. 2010. Understanding internal erosion: a decade of research following a sinkhole event. The International Journal on Hydropower and Dams, **17**(3): 93–98.

Kenney, T.C., and Lau, D. 1985. Internal stability of granular filters. Canadian Geotechnical Journal, **22**(2): 215–225. doi:10.1139/t85-029.

Kenney, T.C., and Lau, D. 1986. Internal stability of granular filters: Reply. Canadian Geotechnical Journal, **23**(3): 420–423. doi:10.1139/t86-068.

Kezdi, A. 1979. Soil physics. Elsevier, Amsterdam.

Li, M., Fannin, R.J., and Garner, S.J. 2009. Application of a new criterion for assessing the susceptibility to internal erosion. *In* Proceedings of the Canadian Dam Association Annual Conference, Whistler, B.C., 3–8 October 2009. Available from www.cda.ca/proceedings%20datafiles/2009/2009-9b-03.pdf [accessed 15 February 2011].

Milligan, V. 1986. Internal stability of granular filters: Discussion. Canadian Geotechnical Journal, **23**(3): 414–418. doi:10.1139/t86-066.

Moffat, R.A. 2005. Experiments on the internal stability of widely graded cohesionless soils. Ph.D. thesis, The University of British Columbia, Vancouver, B.C.

Moffat, R., and Fannin, R.J. 2006. A large permeameter for study of internal stability in cohesionless soils. Geotechnical Testing Journal, **29**(4): 273–279. doi:10.1520/GTJ100021.

Moffat, R., Fannin, R.J., and Garner, S.J. 2011. Spatial and temporal progression of internal erosion in cohesionless soil. Canadian Geotechnical Journal, **48**(3): 399–412. [Companion paper.] doi:10.1139/T10-071.

Muir Wood, D. 2007. The magic of sands — The 20th Bjerrum Lecture presented in Oslo, 25 November 2005. Canadian Geotechnical Journal, **44**(11): 1329–1350. doi:10.1139/T07-060.

Perzlmaier, S., Muckenthaler, P., and Koelewijn, A.R. 2007. Hydraulic criteria for internal erosion in cohesionless soil. *In* Assessment of risk of internal erosion of water retaining structures: dams, dykes and levees. Intermediate Report of the European Working Group of ICOLD. Technical University of Munich, Munich, Germany. pp. 30–44.

Sherard, J.L., and Dunnigan, L.P. 1986. Internal stability of granular filters: Discussion. Canadian Geotechnical Journal, **23**(3): 418–420. doi:10.1139/t86-067.

Sherard, J.L., Dunnigan, L.P., and Talbot, J.R. 1984. Basic properties of sand and gravel filters. Journal of Geotechnical Engineering, ASCE, **110**(6): 684–700. doi:10.1061/(ASCE)0733-9410(1984)110:6(684).

Skempton, A.W., and Brogan, J.M. 1994. Experiments on piping in sandy gravels. Géotechnique, **44**(3): 449–460. doi:10.1680/geot.1994.44.3.449.

Stewart, R.A., and Garner, S.J. 2000. Performance and safety of the

W.A.C. Bennett Dam, a seven year update. *In* Proceedings of the 53rd Canadian Geotechnical Conference, Montréal, Que., 15–18 Oct. 2000. BiTech Publishers Ltd., Richmond, B.C. Vol. 1, pp. 97–105.

Terzaghi, K. 1939. Soil mechanics — a new chapter in engineering science. Journal of the Institution of Civil Engineers, **12**(7): 106–141.

## List of symbols

$D$ particle size diameter
$D_n$ grain size corresponding to $n$% finer (used for the coarser fraction or filter layer)
$D'_{15}$ grain size corresponding to 15% finer (used for the coarser fraction or filter layer)
$d'_{85}$ grain size corresponding to 85% finer (used for the finer fraction or base layer)
$e_c$ void ratio (end-of-consolidation)
$F$ mass fraction smaller than $D$
$H$ mass fraction measured between particles sizes $D$ and $4D$ (Kenney and Lau 1985)
$i$ hydraulic gradient
$i_{av}$ average hydraulic gradient
$i_c$ critical hydraulic gradient
$i_{cr}$ critical hydraulic gradient in zone of instability
$i_{jk}$ hydraulic gradient between ports $j$ and $k$
$\sigma'_v$ vertical effective stress
$\sigma'_{vm}$ average vertical effective stress between two port locations
$\sigma'_{bo}$ bottom vertical effective stress
$\sigma'_{to}$ top vertical effective stress
$\gamma'$ buoyant unit weight
$\gamma_w$ unit weight of water